MATERIALS SCIENCE

Inverse mechanical-swelling coupling of a highly deformed double-network gel

Chika Imaoka[1], Tasuku Nakajima[2,3]*, Tsutomu Indei[2], Masaya Iwata[1,4], Wei Hong[5], Alba Marcellan[6], Jian Ping Gong[2,3]

Mechanical behaviors of a polymer gel are coupled with its swelling behavior. It has been known that typical hydrogels display extension-induced swelling and drying-induced stiffening, called normal mechanical-swelling coupling. In this study, we experimentally found that highly extended double-network (DN) hydrogels exhibit abnormal inverse mechanical-swelling coupling such as extension-induced deswelling and drying-induced softening. We established theoretical hyperelastic and swelling models that reproduced all the complicated mechanical and swelling trends of the highly deformed DN hydrogels. From these theoretical analyses, it is considered that the inverse mechanical-swelling coupling of a DN gel is derived from the extreme nonlinear elasticity of its first network at its ultimate deformation state. These findings contribute toward the understanding of the mechanics of rubber-like materials up to their ultimate deformation and fracture limit.

INTRODUCTION

Elastomers and gels, known as rubber-like materials, are unique soft polymeric materials that allow large and reversible deformation. The elasticity of rubber-like materials regulates their reversible deformability and the environmentally responsive swelling properties of gels (*1*–*3*). Thus, the elasticity of this class of materials constitutes one of the most vital and fundamental topics in polymer science owing to the increased demand for rubber-like materials in industry and biotechnology. The fundamental origin of the elasticity of rubber-like materials is the conformational entropy of their network strands (*1*, *4*). For an adequately small deformation of a rubber-like material, the classical neo-Hookean (NH) hyperelastic model grasps the elasticity and related behaviors of the rubber-like material (*5*). The NH model, also sometimes called Flory's model, assumes that the end-to-end distance of each network strand in a rubber-like material exhibits a Gaussian distribution (*6*). On the other hand, in case a rubber-like material is highly deformed, the end-to-end distance distribution of its strands ceases to follow a Gaussian distribution. Thus, a highly deformed rubber-like material exhibits abnormal responses beyond the predictions of the NH model, such as strongly nonlinear strain hardening (*1*). If a network strand in a rubber-like material attains its maximum allowable deformation, the elasticity of the material is expected to be extremely non-Gaussian. Although numerous hyperelastic models have been proposed for highly deformed rubber-like materials (*7*–*12*), no generally accepted model can completely describe the elasticity of rubber-like materials up to their fracture limit. Primarily, the lack of experimental data on the mechanical properties of rubber-like materials near their "ideal deformation limit" constitutes one of the major reasons. The ideal deformation limit of a rubber-like material can be stated as where (majority of) its network strands attain their maximum allowable deformation. To comprehensively understand the elasticity of rubber-like materials, mechanical data of rubber-like materials up to the ideal deformation limit must be acquired. Nevertheless, the actual deformation limit of a typical rubber-like material is much smaller than the ideal limit, and it is determined by the maximum scale of the internal defects (*13*, *14*). Any rubber-like material originally contains defects of various scales (*15*, *16*), and such defects result in local stress concentration and catastrophic crack propagation in a rubber-like material before attaining its ideal deformation limit (*13*, *17*, *18*). Although the extremely non-Gaussian elasticity of the ultimately stretched network strands should dominate the mechanical responses of the ultimately deformed rubber-like materials, such an effect seldom appears on the elasticity and related phenomena of real rubber-like materials.

In this study, as rubber-like materials that are deformable in the vicinity of the ideal deformation limit of their primary network, we focus on double-network (or multiple-network) materials (called "DN materials"). DN materials are tough and strong rubber-like materials that are characterized by two or more networks with contrasting physical characteristics (*19*, *20*). The primary network of DN materials is brittle (low extensibility) and densely cross-linked with a high modulus, whereas the other networks are highly extensible and sparsely cross-linked with a low modulus. In principle, DN materials can be synthesized from any polymer species if contrasting networks are constructed (*21*). Owing to the large modulus difference between the two networks, the initial mechanical response of the DN materials is dominated by that of the stiff primary network (*22*–*24*). DN materials are known to be extremely insensitive to defects (*25*–*27*) because the contrasting DN structure effectively suppresses the stress concentration at the defects, which has been discussed earlier (*25*, *28*). Owing to this defect insensitivity, in case a DN material is deformed, the primary network in the DN material can be deformed to near its ideal deformation limit without catastrophic failure, whereas the sole first network ruptures much before its ideal extension limit. The deformation of the first network in DN materials to near its ideal limit has been supported by their unique mechanical behaviors such as extreme strain

[1]Graduate School of Life Science, Hokkaido University, Sapporo, Japan. [2]Faculty of Advanced Life Science, Hokkaido University, Sapporo, Japan. [3]Institute for Chemical Reaction Design and Discovery (WPI-ICReDD), Hokkaido University, Sapporo, Japan. [4]NGK Spark Plug Co. Ltd., Nagoya, Aichi, Japan. [5]Department of Mechanics and Aerospace Engineering, Southern University of Science and Technology, 518055 Shenzhen, Guangdong, China. [6]Sciences et Ingénierie de la Matière Molle, ESPCI Paris, Université PSL, CNRS, Sorbonne Université, 75005 Paris, France.
*Corresponding author. Email: tasuku@sci.hokudai.ac.jp

hardening upon extension as a consequence of extreme stiffening of the primary network strands (*23*, *24*, *29*, *30*) and yielding accompanied by massive rupture of the primary network strands (*22*, *31*, *32*). This indicates that the mechanical behavior of an ultimately deformed rubber-like network can be experimentally obtained by embedding it as the primary network in a DN material and deforming it. Such real mechanical data of an ultimately deformed rubber-like material are crucial for investigating and modeling the elasticity of a rubber-like material up to its ultimate deformation and fracture.

As particular experimental data of the ultimately deformed rubber-like materials were obtained through measurements of DN materials, here, we report inverse mechanical-swelling coupling of the DN gels. Generally, the swelling and mechanical behaviors of a gel are coupled (*33*). An example of such coupling, which is termed "mechanical-swelling coupling" hereinafter, is the extension-induced swelling of a conventional gel. Prior researches reported that when a gel at swelling equilibrium is extended in the same solvent, its equilibrium swelling ratio increases further with a decrease in the restoring force (*34*–*36*). Another example of this coupling is the drying-induced stiffening. In case a swollen gel is extended and gradually dried while maintaining its length, the restoring force increases with a decrease in gel volume (*37*). Other examples such as the deswelling of a gel under compressive deformation and the shifting of phase transition temperature of gels by deformation have been reported as well (*38*–*40*). According to theoretical investigations of the mechanical-swelling coupling with the NH model, the extension-induced swelling and drying-induced stiffening have been considered as general behaviors of gels, regardless of their chemical species or detailed network structure (*33*, *37*, *41*, *42*). However, in this study, we experimentally determined that the highly extended DN gels exhibit inverse phenomena: extension-induced "deswelling" and drying-induced "softening," which are the first experimental reports of inverse mechanical-swelling coupling and is beyond the prediction scope of the NH model.

The remainder of this paper is organized as follows. First, we introduce our experimental observations of the inversion of the mechanical-swelling coupling of highly deformed DN gels. Second, we qualitatively explain the origin of the inverse coupling from the extreme nonlinear elasticity of DN gels with the ultimately deformed primary network. Third, we demonstrate that the obtained experimental trends cannot be completely reproduced using existing hyperelastic models for highly deformed rubber-like materials. Last, we propose the hyperelastic model and related swelling model that can explain the trends of the anomalous mechanical-swelling coupling of DN gels.

RESULTS

Preparation of gels

The two-step DN gel preparation process is illustrated in Fig. 1. We first prepared a poly(2-acrylamido-2-methylpropanesulfonic acid sodium salt) (PNaAMPS) network as the primary network and then synthesized a polyacrylamide (PAAm) secondary network within the primary network to obtain the PNaAMPS/PAAm DN gel. The PNaAMPS/PAAm DN gel has been commonly used for fundamental studies of DN materials (*19*, *29*–*31*) (Fig. 1A). In addition, we prepared a PAAm single-network hydrogel (PAAm gel) as the common gel (Fig. 1B). Both gels were soaked in pure water until swelling equilibrium was attained before the measurements. The uniaxial σ-λ curve of the swollen PAAm gel is shown in Fig. 1C, where σ denotes the engineering stress, and λ represents the uniaxial deformation ratio relative to the unloaded state. The σ-λ curve of the PAAm gel until its fracture could be appropriately fitted with the NH model. The σ-λ curve of the swollen PNaAMPS/PAAm DN gel is plotted in Fig. 1D. The DN gel exhibited a much larger stress than the PAAm gel despite containing the PAAm network because the stiff primary network dominated the initial mechanical responses of the DN gel, implying the negligible influence of the soft secondary network on the mechanical response of the DN gel. The high Young's modulus of the DN gel originated from the dense cross-linking of the primary network and the swelling-induced prestretching of the primary network strands during the preparation process (*25*). The σ-λ curve of the DN gel could not be fitted with the NH model at all and displayed extreme strain hardening followed by yielding. This strain hardening originated from the extreme stiffening of the primary network strands of PNaAMPS near their stretching limit, and the yielding point was considered where such primary network strands attained the limit and ruptured (*22*, *23*).

Before the subsequent stress relaxation experiments, the PNaAMPS/PAAm DN gel was subjected to "pretreatment." The aim of the pretreatment is to exclude the effect of strand rupture during the stress relaxation experiments. In case a DN material is extended, a small fraction of the primary network strands (probably shorter ones) ruptures before attaining macroscopic yielding, which appears as irreversible mechanical hysteresis (*29*, *30*). To avoid the occurrence of strand rupture during stress relaxation, we uniaxially pre-extended the DN gel to $\lambda_{pre} = 1.57$ to cut such short strands beforehand, unloaded, and swelled the gel in pure water again. Since such pretreated DN gel already experiences large deformation, no strand rupture is expected when a second deformation smaller than the pretreatment is applied to the gel. Details of the prereatment are described in the Supplementary Materials and fig. S1. Note that we did not apply the pretreatment to the PAAm gel because no internal strand rupture occurs during its extension. Hereafter, the term "the DN gel" corresponds to the pretreated DN gel.

Stress relaxation results under water

First, the PAAm and DN gels were subjected to stress relaxation experiments in water to study extension-induced swelling/deswelling. In particular, the gel at swelling equilibrium in pure water was uniaxially extended to various deformation ratios, λ, and maintained in pure water at a constant length (Fig. 2A). The maximum imposed λ for the DN gel was 1.38, which is smaller than the deformation applied at the pretreatment. The width, $w(t)$, and retraction force of the gels were recorded as a function of time, t. The engineering stress, $\sigma(t)$, is defined as the retraction force divided by the initial cross-sectional area before loading. Thus, the engineering stress defined here is simply proportional to the retraction force without affecting the width variations during stress relaxation.

Upon the stress relaxation of the PAAm gel in water, the width of the extended PAAm gel gradually increased (Fig. 2B) with a reduction in engineering stress, regardless of the imposed λ (Fig. 2C). This means that the extended PAAm gel further swells in water. This extension-induced swelling of a gel during the stress relaxation test in a solvent, which is a typical example of normal mechanical-

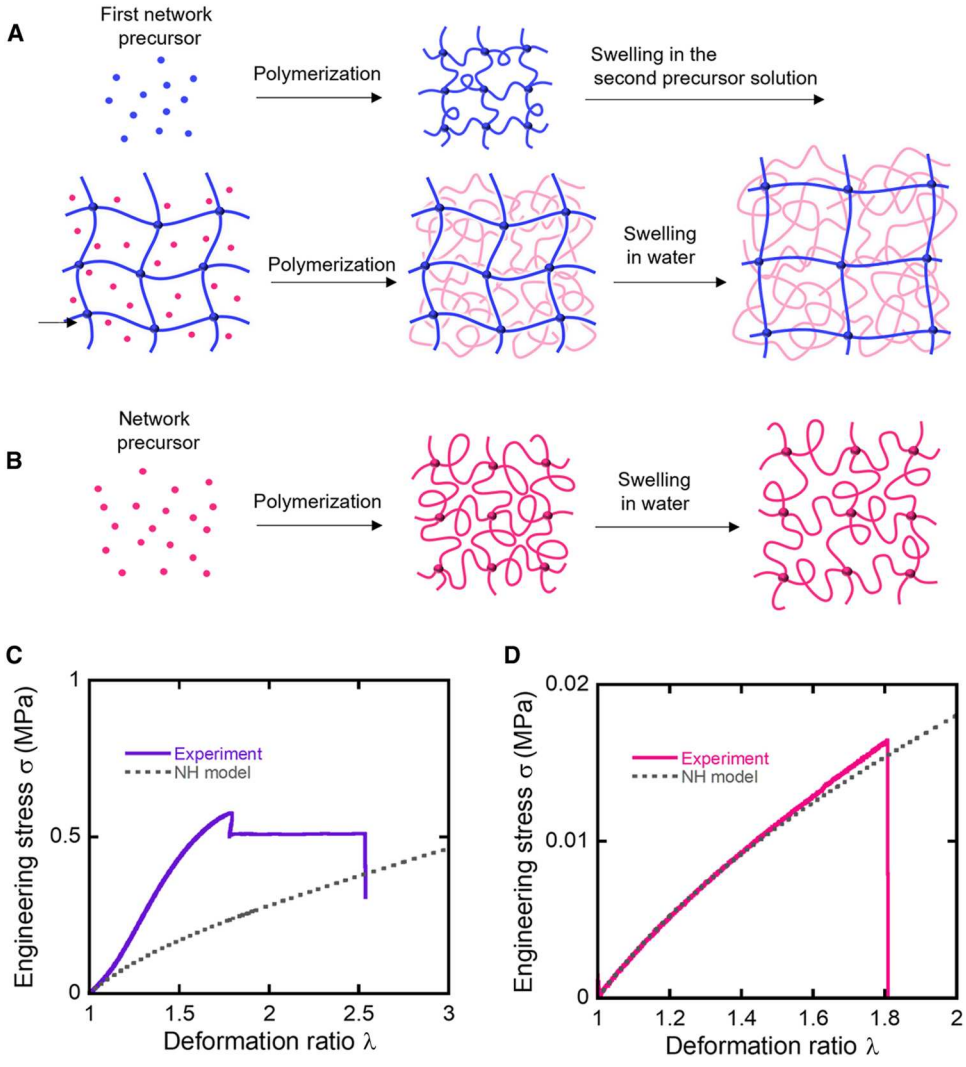

Fig. 1. Preparation and basic mechanical properties of gels. (**A** and **B**) Schematic preparation process of the (A) PNaAMPS/PAAm DN gel and (B) PAAm gel. (**C** and **D**) Uniaxial tensile test results for the (C) PNaAMPS/PAAm DN gel and (D) PAAm gel. Dashed lines represent predictions of the NH model. Parameters in the NH model were determined to reproduce the initial moduli of gels.

swelling coupling, is consistent with prior reports (*33*–*35*). In the case of DN gel, it exhibited similar normal extension-induced swelling if the applied deformation ratio λ is smaller than 1.23 (Fig. 2D). However, in case of imposing a large λ (>1.23), the width of the extended DN gel decreased rather than increased with time, thereby indicating that the highly extended DN gel had abnormal extension-induced deswelling, which is an example of inverse mechanical-swelling coupling. At a threshold λ = 1.23, the width of the DN gel did not vary during the stress relaxation test. During stress relaxation, σ of the DN gel decreased over time regardless of swelling or deswelling (Fig. 2E). This implies that the normal mechanical-swelling coupling of the DN gel at λ < 1.23 can be characterized on the basis of the negative correlation between the swelling ratio and stress, whereas the inverse coupling at λ > 1.23 is characterized by a positive correlation between them.

Subsequently, the equilibrium normalized widths, $w(\infty)/w(0)$, of the extended PAAm and DN gels were extracted for various imposed λ values. To estimate the equilibrium width $w(\infty)$, we adopted $w(100\ \text{min})$ as a value of $w(\infty)$. As depicted in Fig. 3A, $w(\infty)/w(0)$ of the PAAm gel and DN gel at λ < 1.23 was larger than 1, whereas that of the highly deformed DN gel at λ > 1.23 was smaller than 1. On the basis of these data, we calculated the osmotic Poisson's ratio, ν_{os}, of the PAAm and DN gels with various λ values. The ν_{os} of a highly deformable material is defined as $\nu_{os} = -\varepsilon_{trans}/\varepsilon_{tens}$, where ε_{trans} and ε_{tens} denote the true transverse and tensile strains, respectively. As these strains can be expressed using the experimentally obtained parameters, we derived ν_{os} as

$$\nu_{os} = -\frac{\varepsilon_{trans}}{\varepsilon_{tens}} = -\frac{\ln[\lambda^{-0.5} w(\infty)/w(0)]}{\ln\lambda} \quad (1)$$

As a function of λ, the ν_{os} of the extended PAAm and DN gels in water is depicted in Fig. 3B. In the previous work, the ν_{os} of the diluted gel was predicted as 0.25 based on the NH model regardless of the imposed λ (*33*). The ν_{os} of the PAAm gel seems to be consistent with this prediction. In contrast, the ν_{os} of the DN gel was not

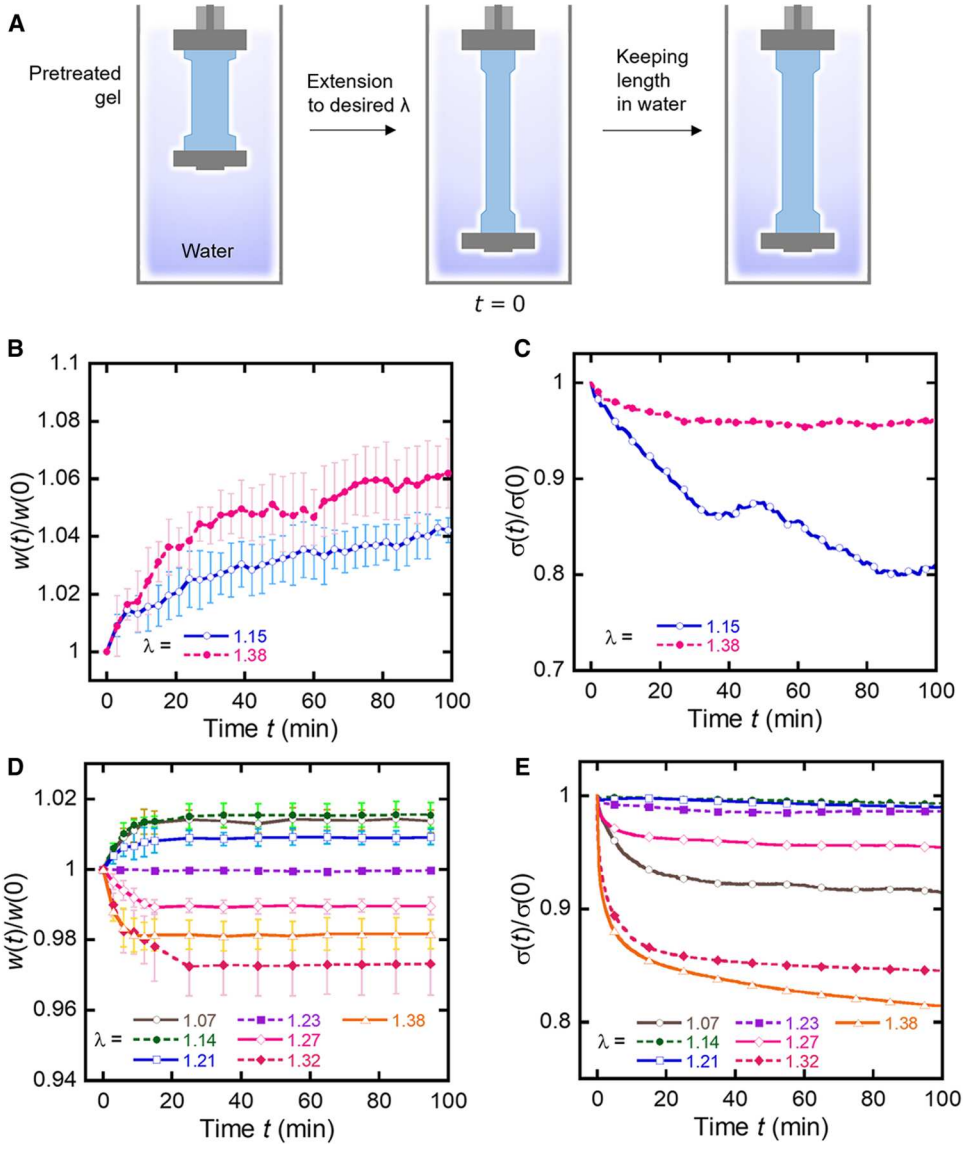

Fig. 2. Stress relaxation in water. (**A**) Experimental setup for stress relaxation under water. (**B**) Normalized width $w(t)/w(0)$ and (**C**) normalized engineering stress $\sigma(t)/\sigma(0)$ of the PAAm gel under water as functions of time. (**D**) $w(t)/w(0)$ and (**E**) $\sigma(t)/\sigma(0)$ of the pretreated PNaAMPS/PAAm DN gel under water as functions of time.

constant but increased with the imposed λ. Last, the ν_{os} of the DN gel exceeded 0.5 at $\lambda > 1.23$ as a consequence of the extension-induced deswelling. Note that the (normal) Poisson's ratio for an isotropic material must not exceed 0.5. A typical material is a closed system that does not allow mass transfer between the system and the outside. In this case, Poisson's ratio must be between −1 and 0.5. In contrast, a gel is a semi-open system that allows solvent transfer from and to the outside. Thus, an osmotic Poisson's ratio of gels greater than 0.5, which corresponds to the extension-induced deswelling, is allowed.

Owing to the extension-induced swelling/deswelling, the volume of the DN gels immediately after the stress relaxation experiment (tested gel, Fig. 4A, ii) changed from that before the experiment (pretreated gel, Fig. 4A, i). To investigate the recovery of the tested DN gels to their original volume, the tested DN gels were immersed in pure water for 24 hours without any external force to form reswollen DN gels (Fig. 4A, iii). We measured the volumes of the pretreated DN gel (i), tested gel (ii), and reswollen gel (iii) as V_a, V_b, and V_a', respectively. Figure 4B shows two volume ratios, V_b/V_a and V_a'/V_a, of the DN gels subjected to the stress relaxation test as a function of λ. In all cases, V_a'/V_a was approximately 1, which signified that the volume of the tested DN gels returned to its original value after free swelling in water. This result suggested that extension-induced swelling/deswelling was not caused by the irreversible modifications in the network structures during the stress relaxation experiment.

Stress relaxation results at 80% RH

We also performed stress relaxation experiments on the PAAm gel and DN gel at 80% relative humidity (RH) to gradually dry the gel during its stress relaxation period (Fig. 5A). As a high relative humidity of 80% ensures steady drying, we assume a nearly

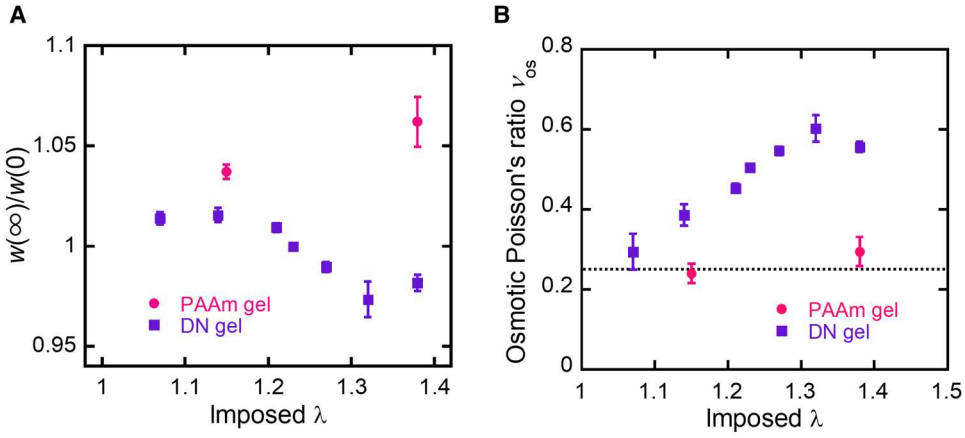

Fig. 3. Swelling equilibrium under tension. (**A**) Equilibrium normalized width, $w(\infty)/w(0)$, and (**B**) osmotic Poisson's ratio, ν_{os}, of the PAAm gel and pretreated PNaAMPS/PAAm DN gel under water as a function of imposed deformation ratio λ. The horizontal dotted line in (B) denotes $\nu_{os} = 0.25$, which is the theoretical ν_{os} of a dilute gel that follows the NH model.

homogeneous water content of the gel during the stress relaxation period. The normalized width of the elongated PAAm gel at 80% RH as a function of time is presented in Fig. 5B. The width of the PAAm gel gradually decreased with time due to the drying. As depicted in Fig. 5C, the engineering stress σ of the PAAm gel increased with decreasing width, regardless of the imposed λ. Such drying-induced stiffening, with a negative correlation between the swelling ratio and stress, is consistent with a previous report (*37*). Similarly, the elongated DN gel was gradually dried during the stress relaxation experiment at 80% RH (Fig. 5D). However, as depicted in Fig. 5E, the σ of the DN gel varied anomalously. For λ = 1.03 (small deformation), the σ of the DN gel increased with drying, similar to common gels. However, for adequately large λ (ultimately deformed), the σ of the DN gel monotonically decreased with drying. Such drying-induced softening with a positive swelling ratio–stress correlation is also an example of inverse mechanical-swelling coupling. At an intermediate λ of 1.07 and 1.13, the stress exhibited a nonmonotonic behavior. At λ = 1.13, the stress initially decreased and thereafter increased as the drying proceeded. Moreover, at λ = 1.07, the time dependence of stress followed a third-order function of t with minimal and maximal values—it increased, decreased, and increased again as drying proceeded, as depicted in Fig. 5F. These nonmonotonic behaviors signified that the drying-induced stiffening and softening of the gel were possibly interchanged under certain conditions.

As discussed earlier, the normal mechanical-swelling coupling was characterized by a negative correlation between the swelling ratio and stress, and vice versa. In Fig. 5 (G to I), the normalized stress $\sigma(t)/\sigma(0)$ is plotted against the normalized width $w(t)/w(0)$. The PAAm gel and DN gel with a small imposed λ displayed a negative correlation, corresponding to the normal mechanical-swelling coupling. The DN gel with a large λ exhibited a positive correlation corresponding to inverse coupling. At intermediate λ such as 1.07, the normal and inverse couplings were complicatedly switched during deswelling.

Incidentally, we confirmed that in case the dried gels were placed at 100% RH, the gel reswelled via reversal on almost the same pathway (fig. S2), thereby demonstrating the reversibility of this process.

Hyperelastic model reproducing inverse coupling

In summary of the experimental results, the highly deformed DN gel exhibited inverse mechanical-swelling couplings (extension-induced deswelling and drying-induced softening). Moreover, we detected complicated switching of the normal and inverse couplings under certain conditions during gel drying. To the best of our knowledge, this is the first experimental observation of inverse mechanical swelling coupling of gels. In this section, we establish a mechanical model to reproduce the inverse coupling to understand the physical origin of the inverse coupling.

First, we propose an ideal representation of the network states for uniaxial stress relaxation experiments that allow volume variations during relaxation, as schematically illustrated in Fig. 6A. The as-prepared network was set as the "reference state" with volume V_0, and the isotropically swollen network was set as the "swollen state" with volume V_a. The swollen network was uniaxially deformed λ times along the x axis to attain the "initial extended state" without volume change. The network at the initial extended state manifested swelling or deswelling at a constant x-axis length to achieve the "state of interest" with volume V_b, which corresponds to the stress relaxation under water or 80% RH. The network at the state of interest was then virtually unloaded with keeping the volume V_b to attain the "virtual unloaded state." The corresponding deformations of the network strands are displayed in Fig. 6B. We adapted this ideal representation to the real stress relaxation experiments of pretreated DN gels. In this case, the network presented in Fig. 6B corresponds to the primary network of the DN gels. As stated earlier, the effect of the soft secondary network on the elasticity is considered to be negligible. Note that the pretreated DN gel was not isotropic but slightly anisotropic after pretreatment; thus, it did not completely correspond to the assumptions in this ideal representation. However, in this study, we assumed that the pretreated DN gel was almost isotropic, and the above ideal network representation was applicable to our system for simplification. For stress relaxation using the DN gel, the as-prepared primary network and pretreated DN gel were set as the reference and swollen states, respectively.

Subsequently, we adapted existing hyperelastic models to this ideal network representation and examined whether these models can reproduce the obtained experimental mechanical-swelling

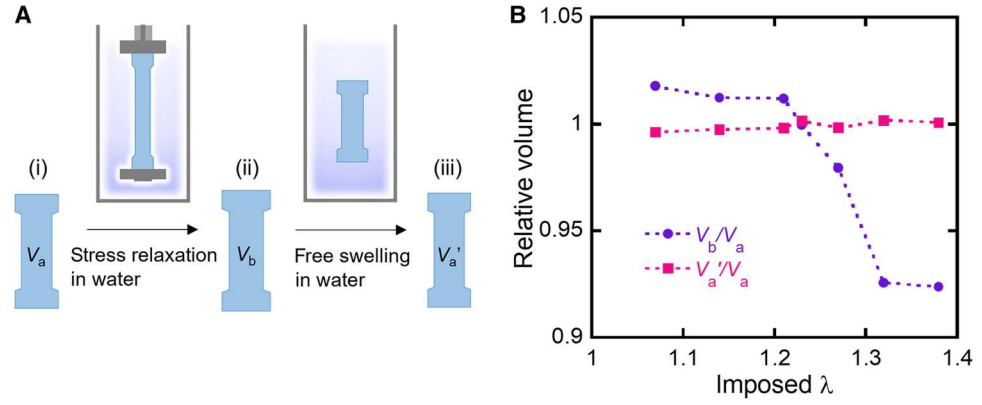

Fig. 4. Reversibility of the swelling process. (**A**) Schematic illustration of gel state and its volume after the stress relaxation experiment and subsequent free swelling. (**B**) Volume ratios V_b/V_a and V_a'/V_a of the DN gels as a function of imposed deformation ratio λ.

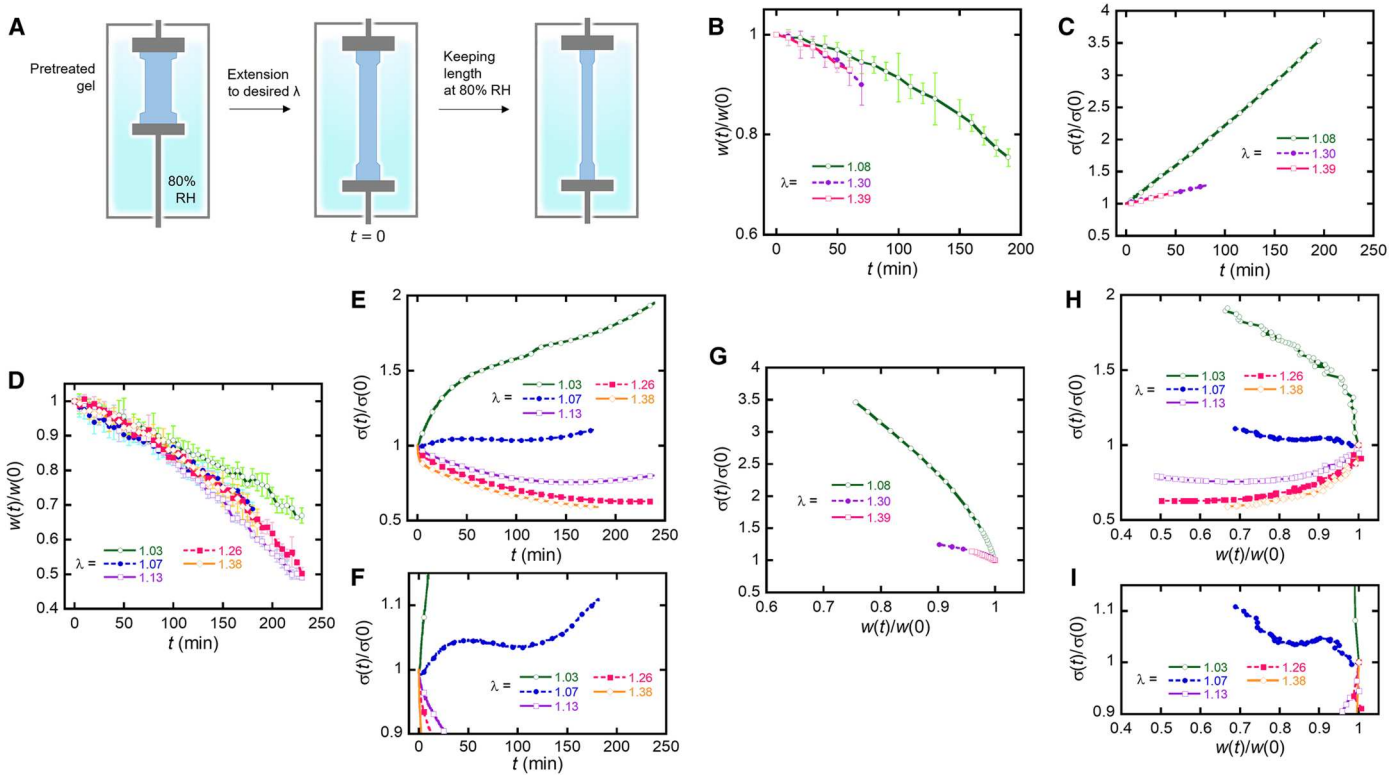

Fig. 5. Stress relaxation at 80% RH. (**A**) Experiment setup. (**B**) $w(t)/w(0)$ and (**C**) $\sigma(t)/\sigma(0)$ of the PAAm gel at 80% RH as functions of time. (**D**) $w(t)/w(0)$ and (**E**) $\sigma(t)/\sigma(0)$ of the pretreated PNaAMPS/PAAm DN gel at 80% RH as functions of time. (**F**) Enlarged version of (E). (**G** and **H**) Relationship between $w(t)/w(0)$ and $\sigma(t)/\sigma(0)$ of the (G) PAAm gel and (H) pretreated PNaAMPS/PAAm DN gel subjected to stress relaxation experiments at 80% RH. (**I**) Enlarged version of (H) near $\sigma(t)/\sigma(0) = 1$.

trends. The data presented in Fig. 5 (G to I) was used as the representative experimental data to be reproduced by the models. For theoretical analyses, the experimentally obtained parameters should be converted into forms that can be theoretically treated with convenience. Regarding deformation, we defined Λ_i as the deformation ratio of the i axis ($i = x, y, z$) of the network relative to its reference state. If we express $\Lambda_{x,y,z}$ at the state of interest using the experimental parameters

$$\Lambda_x \equiv \frac{x_3}{x_0} = \left(\frac{V_a}{V_0}\right)^{1/3} \lambda \tag{2}$$

and

$$\Lambda_y = \Lambda_z \equiv \frac{y_3}{y_0} = \left(\frac{V_a}{V_0}\right)^{1/6} \lambda^{-1/2} \frac{w}{w(0)} \tag{3}$$

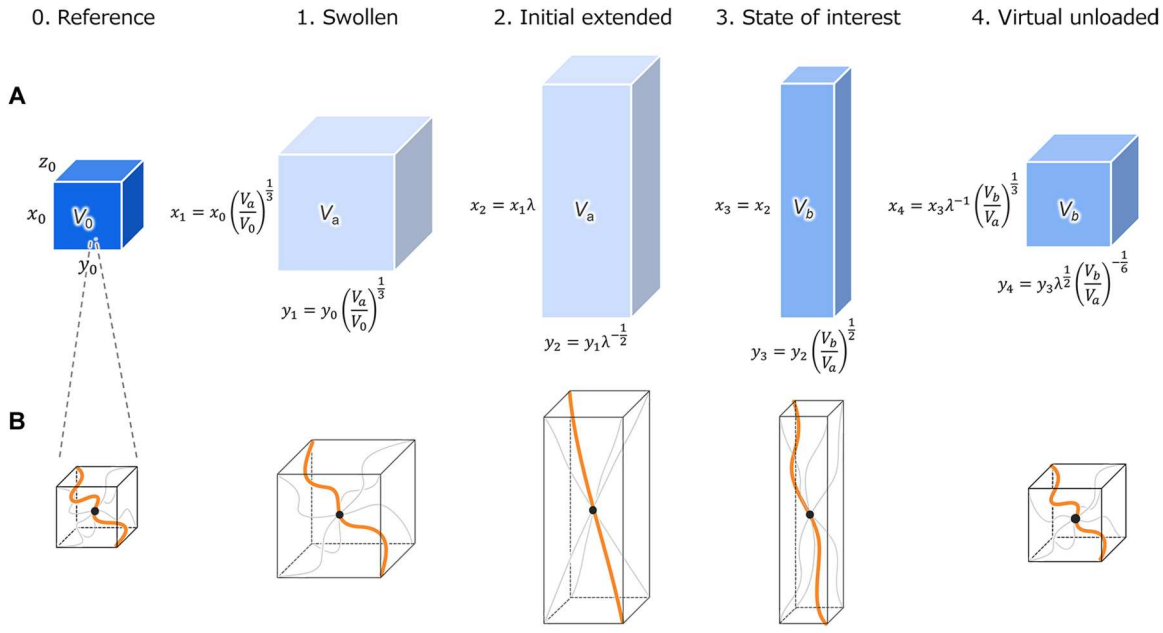

Fig. 6. Ideal states of deformed gels. (**A**) Macroscale and (**B**) molecular scale illustrations of each ideal state in stress relaxation experiments—reference state, swollen state, initial extended state, state of interest, and virtual unloaded state. We illustrate the case of $V_b < V_a$, but $V_b > V_a$ is also allowed.

respectively. In this experiment, the volume ratio of the DN gel to the as-prepared PNaAMPS gel was 10.9:1. Thus, we set $V_a/V_0 = 10.9$ and $(V_a/V_0)^{1/3} \approx 2.2$. Regarding force, we defined the nominal stresses along each axis, σ_i, as the restoring force along each axis divided by the cross-sectional area of the gel at the reference state. According to this definition, σ_x is not equal to the measured engineering stress σ of the gels, but it can be expressed as

$$\sigma_x = \left(\frac{V_a}{V_0}\right)^{2/3}\sigma \tag{4}$$

In addition to these parameters, let ϕ denote the total polymer volume fraction of the gel, and ϕ_0 is ϕ at its reference state.

We assumed that the mixing of the polymer and solvent does not vary the system volume. In addition, we follow the Flory-Rehner–like assumption that the Helmholtz free energy per unit volume of a gel in the reference state, F, can be separated into the osmotic term $F^{os}(\phi)$ and the elastic term $F^{el}(\Lambda_x, \Lambda_y, \Lambda_z)$ (*43*). Under these conditions and assumptions, the variations in F of the gel from its reference state, ΔF, can be expressed as

$$\Delta F = \Delta F^{el} + \Delta F^{os}(\phi) \tag{5}$$

The relative volume of the gel, $\Lambda_x\Lambda_y\Lambda_z$, is inversely proportional to its polymer volume fraction ϕ. Thus

$$\Lambda_x\Lambda_y\Lambda_z = \frac{\phi_0}{\phi}$$

$$\Lambda_y = \Lambda_z = \sqrt{\frac{\phi_0}{\Lambda_x\phi}} \tag{6}$$

The nominal stress σ_i was derived by partially differentiating ΔF with respect to Λ_i. At equilibrium, $\sigma_y = \sigma_z = 0$ under uniaxial deformation. Thus

$$\sigma_x = \frac{\partial \Delta F}{\partial \Lambda_x} = \frac{\partial \Delta F^{el}}{\partial \Lambda_x} + \frac{\partial \Delta F^{os}}{\partial \Lambda_x} = \frac{\partial \Delta F^{el}}{\partial \Lambda_x} - \frac{\phi_0}{{\Lambda_x}^2{\Lambda_y}^2}\left(\frac{\partial \Delta F^{os}}{\partial \phi}\right) \tag{7}$$

$$\sigma_y = \sigma_z = \frac{\partial \Delta F}{\partial \Lambda_y} = \frac{\partial \Delta F^{el}}{\partial \Lambda_y} - \frac{2\phi_0}{\Lambda_x{\Lambda_y}^3}\left(\frac{\partial \Delta F^{os}}{\partial \phi}\right) = 0 \tag{8}$$

The combination of Eqs. 7 and 8 derives the following fundamental equation that dictates axial stress of an uniaxially deformed gel as a function of its deformation

$$\sigma_\gamma = \frac{\partial \Delta F^{el}}{\partial \Lambda_x} - \frac{\Lambda_y}{2\Lambda_y}\frac{\partial \Delta F^{el}}{\partial \Lambda_y} \tag{9}$$

In this study, the variations in the width of the gel during stress relaxation corresponds to a variation in Λ_y at constant Λ_x. The normal mechanical swelling coupling (extension-induced swelling, etc.) corresponds to a reduction in σ_x with an increase in Λ_y, and the inverse coupling corresponds to a reduction in σ_x with a decrease in Λ_y. Thus, the criteria for normal/inverse mechanical-swelling coupling can be stated as

$$\begin{aligned} \left.\frac{\partial \sigma_x}{\partial \Lambda_y}\right|_{\Lambda_x} < 0 &: \text{ normal coupling} \\ \left.\frac{\partial \sigma_x}{\partial \Lambda_y}\right|_{\Lambda_x} > 0 &: \text{ inverse coupling} \end{aligned} \tag{10}$$

Equation 9 can be solved by substituting the function form of ΔF^{el}. In this study, we used various hyperelastic models as ΔF^{el} and verified whether each model reproduces the data in Fig. 5 (G to I). First, we adopted the classical NH model, which assumes an isotropic polymer network composed of network strands with its end-to-end distance distribution following Gaussian statistics (*5*).

ΔF^{el} for the NH model is given as

$$\Delta F^{el} = c_{10}(I_1 - 3) \text{ (NH Model)} \quad (11)$$

where c_{10} is the material constant, and $I_1 = {\Lambda_x}^2 + {\Lambda_y}^2 + {\Lambda_z}^2$ represents the first invariant of the strain tensor (*4*). Substituting Eq. 11 into Eq. 9 results into

$$\sigma_x = 2\left(\Lambda_x - \frac{{\Lambda_y}^2}{\Lambda_x}\right)c_{10} \quad (12)$$

and

$$\left.\frac{\partial \sigma_x}{\partial \Lambda_y}\right|_{\Lambda_x} = -4\frac{\Lambda_y}{\Lambda_x}c_{10} \quad (13)$$

Because c_{10}, Λ_x, and Λ_y must be positive, the right side of Eq. 13 is always negative. It means that the NH model predicts the normal mechanical-swelling coupling at all instances, which does not match our experimental observations for the DN gel.

Second, we apply the Gent model, which is a semi-empirical model frequently adopted to describe the nonlinear elasticity of rubber-like materials (*10*). The Gent model was constructed by replacing $I_1 - 3$ in the NH model with $-J_m \ln\left(1 - \frac{I_1 - 3}{J_m}\right)$ to mathematically express the nonlinear strain hardening of the network strands

$$\Delta F^{el} = -c_{10}J_m \ln\left(1 - \frac{I_1 - 3}{J_m}\right), \text{ (Gent model)} \quad (14)$$

$$\sigma_x = 2\left(\Lambda_x - \frac{{\Lambda_y}^2}{\Lambda_x}\right)c_{10}\frac{J_m}{J_m - I_1 + 3} \quad (15)$$

$$\left.\frac{\partial \sigma_x}{\partial \Lambda_y}\right|_{\Lambda_x} = \frac{4c_{10}J_m\Lambda_y\left[2\left(\Lambda_x - \frac{{\Lambda_y}^2}{\Lambda_x}\right) - \frac{J_m - I_1 + 3}{\Lambda_x}\right]}{(J_m - I_1 + 3)^2} \quad (16)$$

where J_m is the material constant that indicates the maximum allowable $I_1 - 3$. The Gent model exhibits a singularity at $I_1 = J_m + 3$, corresponding to the theoretical deformation limit of the network. Thus, the Gent model is considered suitable for describing the deformation limit of a network (*18*). The Gent model substantially reproduced the uniaxial σ-λ curve of the pretreated DN gel with notable strain hardening (fig. S3). According to Eq. 16, the Gent model predicted monotonical $\sigma_x - \Lambda_y$ relationships at constant Λ_x, wherein the positive or negative slope relied on J_m and Λ_x. Some examples of the $\sigma_x - \Lambda_y$ curves of the Gent model are depicted in fig. S4. For $\Lambda_x < \sqrt{(J_m + 3)/3}$, σ_x monotonically decreased with Λ_y in the physically meaningful Λ_y range, corresponding to normal mechanical-swelling coupling. However, for $\Lambda_x > \sqrt{(J_m + 3)/3}$, σ_x monotonically increased with Λ_y, corresponding to inverse coupling. This means that the Gent model can explain the inverse mechanical-swelling coupling owing to the nonlinearity in the model, which has been pointed out earlier (*44*). At $\Lambda_x = \sqrt{(J_m + 3)/3}$, σ_x is a constant regardless of Λ_y. However, as the Gent model predicts monotonical $\sigma_x - \Lambda_y$ relationships at all instances, the complex stiffening-softening interchange of the DN gel portrayed in Fig. 5I cannot be reproduced by the Gent model.

The failure of the Gent model suggests the inadequacy of its nonlinearity. An appropriate modification of the nonlinearity is required to completely reproduce the experimentally observed stiffening-softening interchange. As an example of such a model, one can add the quadratic term I_1 to the Gent model, such as

$$\Delta F^{el} = -c_{10}J_m \ln\left(1 - \frac{I_1 - 3}{J_m}\right) + c_{20}(I_1 - 3)^2 \text{ (our model)} \quad (17)$$

$$\sigma_x = 2\left(\Lambda_x - \frac{{\Lambda_y}^2}{\Lambda_x}\right)\left[c_{10}\frac{J_m}{J_m - I_1 + 3} + 2c_{20}(I_1 - 3)\right] \quad (18)$$

$$\left.\frac{\partial \sigma_x}{\partial \Lambda_y}\right|_{\Lambda_x} = \frac{4c_{10}J_m\Lambda_y\left[2\left(\Lambda_x - \frac{{\Lambda_y}^2}{\Lambda_x}\right) - \frac{J_m - I_1 + 3}{\Lambda_x}\right]}{(J_m - I_1 + 3)^2} + 8c_{20}\Lambda_y\left[2\left(\Lambda_x - \frac{{\Lambda_y}^2}{\Lambda_x}\right) - \frac{I_1 - 3}{\Lambda_x}\right] \quad (19)$$

The nonlinearity of the proposed model was simply controlled by adjusting the prefactor c_{20} of the added term. By selecting the appropriate values of the coefficients, this model reproduced

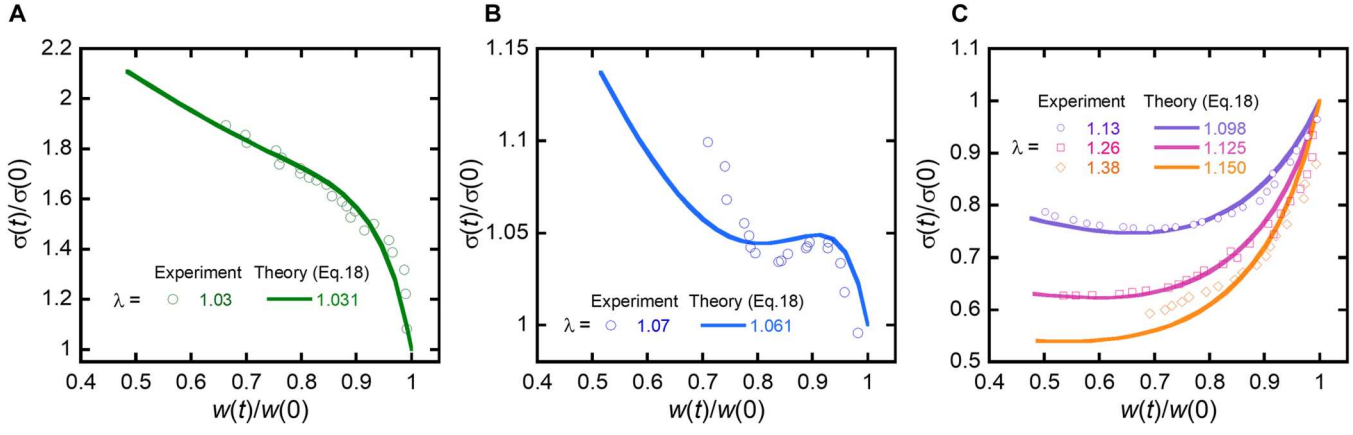

Fig. 7. Model prediction of the stress-width relationship. (**A** to **C**) Experimental and theoretical σ(*t*)/σ(0) of the PNaAMPS/PAAm DN gel as a function of *w*(*t*)/*w*(0) upon the stress relaxation test at 80% RH and at various imposed λ. Symbols and solid lines denote experimental data and model (Eq. 18) predictions, respectively.

almost all the experimental stress relaxation trends of the DN gel. In particular, we set c_{10}, c_{20}, and J_m as 38 kPa, −1.8 kPa, and 14.1, respectively, and, with these coefficients, the uniaxial σ-λ curve of the pretreated DN gel was appropriately reproduced, similar to the Gent model (fig. S3). On the basis of Eq. 18 and these coefficients, we attempted to reproduce the experimental data displayed in Fig. 5 (G to I). To connect the experimental data and the theoretical model, Λ_x, σ_x, and Λ_y in Eq. 18 were replaced by the experimental parameters λ, σ/σ(0), and $w/w(0)$, respectively, using Eqs. 2 to 4. The experimental relationships between σ/σ(0) and $w/w(0)$ of the PNaAMPS/PAAm DN gel subjected to the stress relaxation experiments at 80% RH and corresponding model predictions are depicted in Fig. 7. The model could reproduce the trends in the stress relaxation results for the DN gel at 80% RH. At $1 < \lambda < 1.058$, the theoretical σ/σ(0) monotonically decreased for $w/w(0)$ ranging within $0 < w/w(0) < 1$ (Fig. 7A). At $1.059 < \lambda < 1.072$, two extremal values appeared in the graph (Fig. 7B), and at $1.073 < \lambda < 1.268$, the graph exhibited only one minimal value (Fig. 7C). Moreover, σ/σ(0) monotonically increased with $w/w(0)$ at $1.269 < \lambda$. These trends suitably corresponded with the experimental data, despite a small deviation from the absolute values. The negative c_{20} is vital for reproducing these complex stiffening-softening interchanges.

Swelling model

Furthermore, we also tried to reproduce swelling or deswelling of the pretreated PNaAMPS/PAAm DN gel after the stress relaxation experiment in water by using the general gel swelling model with our hyperelastic model. In case a gel is at its swelling equilibrium, its total swelling pressure Π_{gel} is zero. According to the Flory-Rehner–like assumption, the swelling pressure of a gel is a sum of the osmotic pressure, Π_{os}, and the elastic pressure, Π_{el} (*6*). Specifically, Π_{os} of the DN gel can be separated into polymer-solvent mixing and ionic contributions, as it contains PNaAMPS as a polyelectrolyte (*45*). Upon adopting the classical Flory-Huggins model for a ternary system with two polymer networks and one solvent, the mixing contribution for the DN gel, Π_{mix}, can be expressed as

$$\Pi_{mix} \cong -\frac{kT}{v_s}[\ln(1-\phi_1-\phi_2)+\phi_1+\phi_2-\chi_{12}\phi_1\phi_2 + \chi_{1s}\phi_1(\phi_1+\phi_2)+\chi_{2s}\phi_2(\phi_1+\phi_2)] \quad (20)$$

where k denotes the Boltzmann constant, T denotes the absolute temperature, v_s represents the volume of the water molecule, ϕ_j denotes the volume fraction of each component, and χ_{jk} denotes the Flory interaction parameter between the two components (j or k = 1, 2, or s) (*46*). The subscript 1 denotes PNaAMPS, 2 denotes PAAm, and s indicates water as the solvent. When the solvent does not contain any movable ions like this experimental system, the ionic contribution of the DN gel, Π_{ion}, can be expressed as

$$\Pi_{ion} \cong \frac{\alpha\phi_1}{v_1} \quad (21)$$

where v_1 denotes the volume of the NaAMPS monomeric unit and α indicates the ratio of the mobile counterions to the total counterions in the PNaAMPS network (*46*).

All of the parameters appearing in Eqs. 20 and 21 can be estimated from the experimental data. On the basis of their melt densities, v_s and v_1 have been estimated as 0.03 and 0.2 nm^3, respectively (*47*). The interaction parameters χ_{12}, χ_{1s}, and χ_{2s} have been determined by neutron scattering experiments as 0.015, 0.3, and 0.45, respectively (*47*), wherein α has been estimated by the swelling study as 0.238 (*46*). For the determination of ϕ_1 and ϕ_2, which are functions of the gel volume, we first estimate the volume fractions of PNaAMPS and PAAm in the DN gel at the swollen state, which are defined as Φ_1 and Φ_2, as 0.0152 and 0.0723, respectively, based on the preparation conditions and swelling ratios (Supplementary Materials). Under constant Λ_x, ϕ_1 and ϕ_2 at the state of interest vary with w as $\phi_1 = \Phi_1[w/w(0)]^{-1/2}$ and $\phi_2 = \Phi_2[w/w(0)]^{-1/2}$.

On the contrary, Π_{el} was evaluated by differentiating ΔF_{el} with respect to the relative gel volume to obtain

$$\Pi_{el} = -\frac{\partial \Delta F^{el}}{\partial(V/V_0)} \quad (22)$$

In the reported stress relaxation test, the variations in the elastic energy and volume of the gel occur as a consequence of the variations in Λ_y with constant Λ_x. Thus

$$\Pi_{el} = -\frac{\partial \Delta F^{el}}{\partial \Lambda_y}\frac{\partial \Lambda_y}{\partial(V/V_0)}\bigg|_{\Lambda_x} \quad (23)$$

We adopted the proposed model (Eq. 17) as an elastic energy density function. Upon substituting Eq. 17 into Eq. 23 and performing the differentiations, we obtained the elastic pressure of the DN gel after stress relaxation as follows

$$\Pi_{el} = -2\Lambda_x^{-1}\left[c_{10}\frac{J_m}{J_m - I_1 + 3} + 2c_{20}(I_1 - 3)\right] \text{ (our model)} \quad (24)$$

The DN gel subjected to the stress relaxation experiment in water attained its swelling equilibrium upon satisfying the following equation

$$-2\Lambda_x^{-1}\left[c_{10}\frac{J_m}{J_m - I_1 + 3} + 2c_{20}(I_1 - 3)\right] - \frac{kT}{v_s}[\ln(1-\phi_1-\phi_2)+\phi_1+\phi_2-\chi_{12}\phi_1\phi_2+\chi_{1s}\phi_1(\phi_1+\phi_2) + \chi_{2s}\phi_2(\phi_1+\phi_2)] + \frac{\alpha\phi_1}{v_1} = 0 \quad (25)$$

where $\phi_1 = \Phi_1[w/w(0)]^{-1/2}$ and $\phi_2 = \Phi_2[w/w(0)]^{-1/2}$.

By using Eq. 25, the equilibrium-normalized width $w(\infty)/w(0)$ of the DN gel subjected to stress relaxation in water as a function of imposed λ can be estimated. For the calculation, Λ_x and Λ_y in Eq. 25 were replaced by λ and $w/w(0)$ based on Eqs. 2 and 3, the constants for Π_{os} (v_s, v_1, α, χ_{12}, χ_{1s}, χ_{2s}, Φ_1, and Φ_2) were determined as stated earlier, and the constants for Π_{el} (c_{10}, c_{20}, and J_m) were identical to those used in Fig. 7. The evaluation results are depicted using solid lines in Fig. 8. At $\lambda < 1.25$, the model predicted that $w(\infty)/w(0) > 1$, corresponding to extension-induced swelling and normal coupling. On the other hand, at $\lambda > 1.26$, the model predicted $w(\infty)/w(0) < 1$, corresponding to extension-induced deswelling and inverse coupling. These trends are consistent with the stress relaxation test results of the DN gel in water. On the other hand, the predicted $w(\infty)/w(0)$ at $\lambda = 1$ was not equal to 1, which did not satisfy the

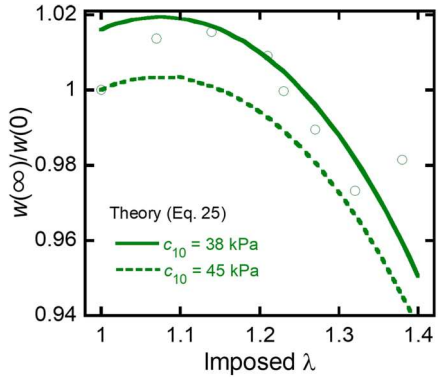

Fig. 8. Model prediction of the equilibrium swelling state. Experimental and theoretical $w(\infty)/w(0)$ of the PNaAMPS/PAAm DN gel as a function of imposed λ during stress relaxation test under water. Circle symbols and lines denote experimental data and model (Eq. 25) predictions, respectively.

physical requirement. For c_{10} = 45 kPa instead of 38 kPa (dashed line in Fig. 8), the model predicted a similar curve and $w(\infty)/w(0) = 1$ at $\lambda = 1$, despite the slight deviation of the absolute $w(\infty)/w(0)$ from the experimental value. This theoretically observed transition from normal to inverse coupling is the consequence of strong nonlinearity in the hyperelastic model. If the NH model that did not consider the strong nonlinearity is adopted for derivation of Eq. 25, such swelling model predicted the extension-induced swelling at all instances (fig. S5), which does not match our results for the DN gels.

We also adopted alternative hyperelastic models such as the Mooney-Rivlin (*8*), Arruda-Boyce (*9*), Yeoh (*10*), and extended Gent models (*48*), and examined whether each model reproduces the mechanical trends of DN gels. The equation forms of these models are provided in the Supplementary Materials. The results are summarized in Table 1. None of them can reproduce all the characteristic mechanical trends of DN gels owing to the inappropriate modeling of the nonlinearity of the network.

Table 1. Applicability of each hyperelastic model. The table summarizes whether each hyperelastic model can express a characteristic mechanical trend of the measured DN gel or not; possible (○) and not possible (–).

	Describing the deformation limit	Inverse coupling when highly deformed	Stiffening-softening interchange during the drying
Neo-Hookean	–	–	–
Mooney-Rivlin	–	–	–
Gent	○	○	–
Arruda-Boyce	○	○	–
Yeoh	–	○	○
Extended Gent	○	○	–
Our model	○	○	○

DISCUSSION

The developed hyperelastic and swelling models appropriately described the trends of the mechanical-swelling coupling of the DN gels. However, the limitation of the current models is that they cannot reproduce the absolute experimental values, which is potentially because of three possible reasons. The first reason is the simplicity of the proposed hyperelastic model. Here, a hyperelastic model (Eq. 17) was constructed by modifying the Gent model using only a single quadratic term of I_1. The introduction of additional correction terms may produce theoretical values that are proximate to the experimental results. The second reason pertains to the anisotropy of the pretreated DN gel, which was not considered in the models. Upon pretreatment (uniaxial extension) of the DN gel, its primary network strands along the tensile axis get damaged, but those along other axes remain intact, which leads to anisotropy of the pretreated DN gel. For example, the modulus of the pretreated DN gel along the x axis is expected to be smaller than that along y and z axes due to the anisotropic mechanical damage (*30*). The DN gel subjected to the pretreatment also exhibits anisotropic swelling: It slightly swelled (1.14 times) along the stretching axis but negligibly swelled (1.00 times) along the other two axes in water. While the effect of these anisotropies on the mechanical-swelling coupling can be considered to be not crucial, anisotropic hyperelastic and swelling models are desired to precisely reproduce the results of anisotropic pretreated DN gels. The third reason is accounted for by the inhomogeneity of the DN gels. Since the first network was prepared via random copolymerization of monomers and cross-linkers, the network contained inhomogeneities of various types and scales, as cited in previous studies (*16*, *49*). To avoid the effect of inhomogeneity, a DN gel with a defect-free primary network such as a tetra-PEG network is desirable for future studies (*50*). Furthermore, the dependence of the elasticity of the ultimately deformed networks on the chemical species should be investigated as well. Reportedly, the elasticity of single polymer chain at its ultimately stretched state strongly relies on its chemical species (*51*, *52*) because the deformation of the chemical bonds influenced the elasticity of an ultimately stretched polymer chain in addition to the conformational entropy. Therefore, the same stress relaxation experiments should be performed on DN gels with the primary network of various chemical species for a comparative analysis of the results.

In conclusion, inverse mechanical-swelling coupling was observed for highly deformed PNaAMPS/PAAm DN hydrogels, where the primary network strands were ultimately stretched and exhibited extreme nonlinear elasticity. All experimental trends of the stress-width relationship can be reproduced by the proposed hyperelastic model constructed by adding the quadratic term I_1 to the Gent model. In addition, extension-induced deswelling was reproduced by a combination of the proposed hyperelastic model and swelling theory of DN gels. This research can contribute to the understanding of large deformation of rubbery materials from the following two viewpoints. First, this study provides a strategy to deform a real polymer network to its ideal deformation limit. As discussed in the Introduction, a typical real polymer network breaks much before its ideal limit when deformed. On the other hand, a polymer network embedded in a DN gel as the first network can be deformed close to its ideal limit without being affected by the defect. Second, analysis of the mechanical-swelling

coupling can lead to more precise elastic models for rubbery materials. Since the elastic stress-strain relationships of a rubbery material are derived from its strain energy density function, estimation of accurate strain energy density function form is necessary to understand its various mechanical responses. Researchers usually adopt uniaxial or biaxial extension tests for the estimation, but these tests only show few facets of the mechanical behavior of the rubbery material. Here, our stress relaxation tests can be regarded as uniaxial confined biaxial deformation test. Mechanical data from such an unnoticed deformation mode makes the strain energy density function more appropriate. We showed that most of the proposed phenomenological models cannot reproduce the obtained mechanical-swelling coupling of the DN gel, but our model can do. Further experiments on mechanical-swelling coupling and its analyses can lead to a more precise strain energy density function of rubbery materials. Moreover, this study aids in understanding the behavior of DN materials under large mechanical loads. Various applications of DN materials have been anticipated under heavy loads, such as artificial knee cartilage working under a stress of >10 MPa (*53*). Thus, the unique mechanical-swelling coupling of DN materials revealed by this study will promote the investigation of DN materials used in severe mechanical environments.

MATERIALS AND METHODS

Materials

Acrylamide (AAm), divinylbenzene (DVB; mixture of isomers), *N*,*N*′-methylenebisacrylamide (MBAA), 2-oxoglutaric acid (α-keto), potassium peroxodisulfate (KPS), *N*,*N*,*N*′,*N*′-tetramethylethylenediamine (TEMED), and *N*,*N*-dimethylformamide (DMF) were procured from FUJIFILM Wako Pure Chemical Corporation Inc., Japan, and 2-acrylamido-2-methylpropanesulfonic acid sodium salt (NaAMPS) was procured from Toa Gosei Co. Ltd., Japan. AAm was recrystallized from acetone, and all other chemicals were used without further purification.

Synthesis of DN gels

PNaAMPS/PAAm DN gels were synthesized via sequential free-radical polymerization. Initially, 20 ml of the first network precursor solution was prepared by mixing 1.4 M NaAMPS as the monomer, 56 mM DVB as the cross-linker, 14 mM α-keto as the initiator, 9 ml of DMF, and pure water. The solution was poured into molds formed by two soda-lime glass plates (thickness: 3 mm) and separated by a U-shaped silicone rubber spacer (thickness: 0.5 mm). Thereafter, the molds were irradiated with 365-nm intense ultraviolet (UV; 340 mW/cm^2) for 30 min and maintained under ambient conditions (around 25°C) for 1 day to prepare the PNaAMPS gels. Subsequently, the obtained PNaAMPS gels were immersed in an excess second network precursor aqueous solution containing 2 M AAm as the monomer, 4×10^{-4} M MBAA as the cross-linker, and 4×10^{-4} M α-keto as the initiator for 1 day. After attaining swelling equilibrium, the gels were sandwiched between two glass plates and transferred to an argon blanket. The DN gels were prepared by irradiation with 365-nm UV (4 mW/cm^2) for 8 hours to synthesize the PAAm network in the presence of the PNaAMPS network. The obtained DN gels were immersed in excess pure water for at least 1 day to remove any unreacted reagents and attain the initial swelling equilibrium.

Synthesis of PAAm gels

The gel precursor aqueous solution was prepared by mixing 2 M AAm as the monomer, 20 mM MBAA as the cross-linker, 5 mM KPS as the initiator, and 5 mM TEMED as the accelerator with pure water. The solution was poured into the molds formed by two soda-lime glass plates separated by a U-shaped silicone rubber spacer (thickness: 1 mm) and maintained for 1 day at 4°C to prepare the PAAm gels. The obtained PAAm gels were immersed in excess pure water for at least 1 day to remove any unreacted reagents and attain the swelling equilibrium.

Uniaxial tensile tests

The swollen gels were cut into dumbbell shapes (gauge length: 35 mm; width: 10 mm). Uniaxial tensile tests were performed using a tensile tester Instron 5965 equipped with a noncontact video extensometer (AVE; Instron Co.). The tensile velocity was set at 100 mm/min. The engineering stress, σ, was defined as the force divided by the cross-sectional area of the specimen before extension. The deformation ratio, λ, was defined as the current gauge length divided by the original gauge length. A representative stress-deformation relationship among three measurements is shown in the graphs.

Pretreatment of gels for stress relaxation tests

The swollen DN gels were cut into dumbbell shapes (gauge length: 35 mm; width: 10 mm). The DN gel specimen was preextended to $\lambda_{pre} = 1.57$ and immediately unloaded with a tensile velocity of 100 mm/min. Subsequently, the specimen was removed from the tester and immersed in pure water for 1 day to enable it to attain another swelling equilibrium. The swollen PAAm gels were cut into the same dumbbell shape (gauge length: 35 mm; width: 10 mm). No pre-extension was applied to the PAAm gel specimens. Periodic dots with black ink (1.5 mm × 1.5 mm) were stamped on the preextended DN gel specimens and PAAm gel specimens to analyze their (longitudinal) deformation ratio, λ, and the normalized width, $w(t)/w(0)$, during the subsequent stress relaxation tests (fig. S6).

Stress relaxation tests under water

The pretreated DN gel or PAAm gel specimen was set to a tensile tester Tensilon RTG-1310 (Orientec Co.) equipped with a water bath. The specimen was attached to the tester in a water bath and uniaxially extended to the desired length with a tensile velocity of 100 mm/min to achieve a constant longitudinal length in a water bath. Owing to the sufficiently fast tensile velocity, the swelling/deswelling of the specimen during loading was negligible. The engineering stress $\sigma(t)$ and normalized width $w(t)/w(0)$ of the specimen were investigated as a function of time t. $t = 0$ was set when the specimen reaches the desired length. Note that $\sigma(t)$ is defined as the restoring force divided by the cross-sectional area of the specimen before extension; thus, change in the cross-sectional area by lateral swelling/deswelling during stress relaxation need not be considered in the calculation of σ. The data are from single experiments. The $w(t)/w(0)$ of the specimen was determined by capturing images of the specimen using a camera EOS 90D (Canon Inc.) and analyzing the distances between the dots on the specimen. We selected four pairs of the stamped dots near the center of the specimen and measured the distance between them manually using ImageJ. The error bars in the graphs represent the standard deviation in measurements of four different pairs within the same sample. λ of the

extended specimen was similarly determined by analysis of the distance of the dots.

Stress relaxation tests at 80% RH

The pretreated specimen was set to a tensile tester SHIMADZU AG-Xplus (Shimadzu Co.) equipped with a humidity and temperature testing chamber. Before the test, the temperature and relative humidity in the chamber were preset as 25°C and 80% RH, respectively. The specimen was set to the tester in the testing chamber, extended to the desired deformation ratio λ with a tensile velocity of 100 mm/min to maintain its constant longitudinal length at 25°C, 80% RH. As the tensile velocity was sufficiently large, the drying of the specimen during loading was negligible. The $\sigma(t)$ and $w(t)/w(0)$ of the specimen were analyzed as a function of time t in the same manner. The data are from single experiments.

Supplementary Materials

This PDF file includes:

Supplementary Text
Figs. S1 to S6

REFERENCES AND NOTES

1. L. R. G. Treloar, *The Physics of Rubber Elasticity* (Oxford Univ. Press, 1975).
2. M. Quesada-Pérez, J. A. Maroto-Centeno, J. Forcada, R. Hidalgo-Alvarez, Gel swelling theories: The classical formalism and recent approaches. *Soft Matter* **7**, 10536–10547 (2011).
3. M. C. Koetting, J. T. Peters, S. D. Steichen, N. A. Peppas, Stimulus-responsive hydrogels: Theory, modern advances, and applications. *Mater. Sci. Eng. R Rep.* **93**, 1–49 (2015).
4. R. L. Anthony, R. H. Caston, E. Guth, Equations of state for natural and synthetic rubber-like materials. I. Unaccelerated natural soft rubber. *J. Phys. Chem.* **46**, 826–840 (1942).
5. L. R. G. Treloar, The elasticity of a network of long-chain molecules—II. *Trans. Faraday Soc.* **39**, 241–246 (1943).
6. M. Rubinstein, R. H. Colby, *Polymer Physics* (Oxford Univ. Press, 2003).
7. M. Hossain, P. Steinmann, More hyperelastic models for rubber-like materials: Consistent tangent operators and comparative study. *J. Mech. Behav. Mater.* **22**, 27–50 (2013).
8. M. Mooney, A theory of large elastic deformation. *J. Appl. Phys.* **11**, 582–592 (1940).
9. E. M. Arruda, M. C. Boyce, A three-dimensional constitutive model for the large stretch behavior of rubber elastic materials. *J. Mech. Phys. Solids* **41**, 389–412 (1993).
10. O. H. Yeoh, Some forms of the strain energy function for rubber. *Rubber Chem. Technol.* **66**, 754–771 (1993).
11. A. N. Gent, A new constitutive relation for rubber. *Rubber Chem. Technol.* **69**, 59–61 (1996).
12. H.-G. Kilian, Equation of state of real networks. *Polymer* **22**, 209–217 (1981).
13. C. Chen, Z. Wang, Z. Suo, Flaw sensitivity of highly stretchable materials. *Extrem. Mech. Lett.* **10**, 50–57 (2017).
14. C. Creton, 50th anniversary perspective: Networks and gels: Soft but dynamic and tough. *Macromolecules* **50**, 8297–8316 (2017).
15. W. Gronski, R. Stadler, M. M. Jacobi, Evidence of nonaffine and inhomogeneous deformation of network chains in strained rubber-elastic networks by deuterium magnetic resonance. *Macromolecules* **17**, 741–748 (1984).
16. M. Shibayama, Spatial inhomogeneity and dynamic fluctuations of polymer gels. *Macromol. Chem. Phys.* **199**, 1–30 (1998).
17. A. Sugimura, M. Asai, T. Matsunaga, Y. Akagi, T. Sakai, H. Noguchi, M. Shibayama, Mechanical properties of a polymer network of Tetra-PEG gel. *Polym. J.* **45**, 300–306 (2012).
18. Y. Akagi, T. Katashima, H. Sakurai, U.-I. Chung, T. Sakai, Ultimate elongation of polymer gels with controlled network structure. *RSC Adv.* **3**, 13251–13258 (2013).
19. J. P. Gong, Y. Katsuyama, T. Kurokawa, Y. Osada, Double-network hydrogels with extremely high mechanical strength. *Adv. Mater.* **15**, 1155–1158 (2003).
20. E. Ducrot, Y. Chen, M. Bulters, R. P. Sijbesma, C. Creton, Toughening elastomers with sacrificial bonds and watching them break. *Science* **344**, 186–189 (2014).
21. T. Nakajima, H. Sato, Y. Zhao, S. Kawahara, T. Kurokawa, K. Sugahara, J. P. Gong, A universal molecular stent method to toughen any hydrogels based on double network concept. *Adv. Funct. Mater.* **22**, 4426–4432 (2012).
22. T. Matsuda, T. Nakajima, Y. Fukuda, W. Hong, T. Sakai, T. Kurokawa, U.-I. Chung, J. P. Gong, Yielding criteria of double network hydrogels. *Macromolecules* **49**, 1865–1872 (2016).
23. E. Ducrot, C. Creton, Characterizing large strain elasticity of brittle elastomeric networks by embedding them in a soft extensible matrix. *Adv. Funct. Mater.* **26**, 2482–2492 (2016).
24. P. Millereau, E. Ducrot, J. M. Clough, M. E. Wiseman, H. R. Brown, R. P. Sijbesma, C. Creton, Mechanics of elastomeric molecular composites. *Proc. Natl. Acad. Sci. U.S.A.* **115**, 9110–9115 (2018).
25. J. P. Gong, Why are double network hydrogels so tough? *Soft Matter* **6**, 2583–2590 (2010).
26. W. Zhang, X. Liu, J. Wang, J. Tang, J. Hu, T. Lu, Z. Suo, Fatigue of double-network hydrogels. *Eng. Fract. Mech.* **187**, 74–93 (2018).
27. Y. Zhang, K. Fukao, T. Matsuda, T. Nakajima, K. Tsunoda, T. Kurokawa, J. P. Gong, Unique crack propagation of double network hydrogels under high stretch. *Extrem. Mech. Lett.* **51**, 101588 (2022).
28. X. Zhao, A theory for large deformation and damage of interpenetrating polymer networks. *J. Mech. Phys. Solids* **60**, 319–332 (2012).
29. T. Nakajima, T. Kurokawa, S. Ahmed, W.-L. Wu, J. P. Gong, Characterization of internal fracture process of double network hydrogels under uniaxial elongation. *Soft Matter* **9**, 1955–1966 (2013).
30. T.-T. Mai, T. Matsuda, T. Nakajima, J. P. Gong, K. Urayama, Distinctive characteristics of internal fracture in tough double network hydrogels revealed by various modes of stretching. *Macromolecules* **51**, 5245–5257 (2018).
31. Y.-H. Na, Y. Tanaka, Y. Kawauchi, H. Furukawa, T. Sumiyoshi, J. P. Gong, Y. Osada, Necking phenomenon of double-network gels. *Macromolecules* **39**, 4641–4645 (2006).
32. T. Matsuda, R. Kawakami, R. Namba, T. Nakajima, J. P. Gong, Mechanoresponsive self-growing hydrogels inspired by muscle training. *Science* **363**, 504–508 (2019).
33. K. Urayama, T. Takigawa, Volume of polymer gels coupled to deformation. *Soft Matter* **8**, 8017–8029 (2012).
34. T. Takigawa, K. Urayama, Y. Morino, T. Masuda, Simultaneous swelling and stress relaxation behavior of uniaxially stretched polymer gels. *Polym. J.* **25**, 929–937 (1993).
35. M. Fujine, T. Takigawa, K. Urayama, Strain-driven swelling and accompanying stress reduction in polymer gels under biaxial stretching. *Macromolecules* **48**, 3622–3628 (2015).
36. P. Chiarelli, P. J. Basser, D. Derossi, S. Goldstein, The dynamics of a hydrogel strip. *Biorheology* **29**, 383–398 (1992).
37. R. H. Pritchard, E. M. Terentjev, Swelling and de-swelling of gels under external elastic deformation. *Polymer* **54**, 6954–6960 (2013).
38. E. Geissler, A. M. Hecht, F. Horkay, M. Zrinyi, Compressional modulus of swollen polyacrylamide networks. *Macromolecules* **21**, 2594–2599 (1988).
39. A. Suzuki, K. Sanda, Y. Omori, Phase transition in strongly stretched polymer gels. *J. Chem. Phys.* **107**, 5179–5185 (1997).
40. P. Pekarski, A. Tkachenko, Y. Rabin, Deformation-induced anomalous swelling of topologically disordered gels. *Macromolecules* **27**, 7192–7196 (1994).
41. W. Hong, X. Zhao, J. Zhou, Z. Suo, A theory of coupled diffusion and large deformation in polymeric gels. *J. Mech. Phys. Solids* **56**, 1779–1793 (2008).
42. M. Doi, Gel dynamics. *J. Phys. Soc. Jpn.* **78**, 052001 (2009).
43. P. J. Flory, J. Rehner Jr., Statistical mechanics of cross-linked polymer networks II. Swelling. *J. Chem. Phys.* **11**, 521–526 (1943).
44. D. Okumura, S. A. Chester, Ultimate swelling described by limiting chain extensibility of swollen elastomers. *Int. J. Mech. Sci.* **144**, 531–539 (2018).
45. J. Ri˘ka, T. Tanaka, Swelling of ionic gels: Quantitative performance of the Donnan theory. *Macromolecules* **17**, 2916–2921 (1984).
46. T. Nakajima, T. Chida, K. Mito, T. Kurokawa, J. P. Gong, Double-network gels as polyelectrolyte gels with salt-insensitive swelling properties. *Soft Matter* **16**, 5487–5496 (2020).
47. T. Tominaga, V. R. Tirumala, S. Lee, E. K. Lin, J. P. Gong, W.-L. Wu, Thermodynamic interactions in double-network hydrogels. *J. Phys. Chem. B* **112**, 3903–3909 (2008).
48. T. Katashima, K. Urayama, U. Chung, T. Sakai, Strain energy density function of a near-ideal polymer network estimated by biaxial deformation of Tetra-PEG gel. *Soft Matter* **8**, 8217–8222 (2012).
49. E. Sato-Matsuo, M. Orkisz, S.-T. Sun, Y. Li, T. Tanaka, Origin of structural inhomogeneities in polymer gels. *Macromolecules* **27**, 6791–6796 (1994).
50. T. Nakajima, Y. Fukuda, T. Kurokawa, T. Sakai, U. Chung, J. P. Gong, Synthesis and fracture process analysis of double network hydrogels with a well-defined first network. *ACS Macro Lett.* **2**, 518–521 (2013).
51. X. Zhang, C. Liu, Z. Wang, Force spectroscopy of polymers: Studying on intramolecular and intermolecular interactions in single molecular level. *Polymer* **49**, 3353–3361 (2008).
52. T. Hugel, M. Rief, M. Seitz, H. E. Gaub, R. R. Netz, Highly stretched single polymers: Atomic-force-microscope experiments versus ab-initio theory. *Phys. Rev. Lett.* **94**, 048301 (2005).
53. T. Nonoyama, J. P. Gong, Tough double network hydrogel and its biomedical applications. *Annu. Rev. Chem. Biomol. Eng.* **12**, 393–410 (2021).

Acknowledgments: We thank Y. Katsuyama, M. Matsumoto, and M. Matsushita (Hokkaido University) for help with experiments. The Institute for Chemical Reaction Design and Discovery (WPI-ICReDD) was established by the World Premier International Research Initiative (WPI), MEXT, Japan. **Funding:** This work was supported by JSPS KAKENHI (grant numbers 17H04891 and 22H04968) and JST, PRESTO (grant number JPMJPR2098). **Author contributions:** Conceptualization: T.N. and A.M. Methodology: C.I., T.N., and M.I. Experiments: C.I. Theoretical investigation: W.H., T.N., C.I., and T.I. Supervision: T.N. and J.P.G. Writing—original draft: T.N. and C.I. Writing—review and editing: T.N., T.I., A.M., W.H., and J.P.G. **Competing interests:** The authors declare that they have no competing interests. **Data and materials availability:** All data needed to evaluate the conclusions in the paper are present in the paper and/or the Supplementary Materials.

Submitted 13 December 2022
Accepted 6 April 2023
Published 10 May 2023
10.1126/sciadv.abp8351

ScienceAdvances

Inverse mechanical-swelling coupling of a highly deformed double-network gel

Chika Imaoka, Tasuku Nakajima, Tsutomu Indei, Masaya Iwata, Wei Hong, Alba Marcellan, and Jian Ping Gong

Sci. Adv., **9** (19), eabp8351.
DOI: 10.1126/sciadv.abp8351